Hindawi
Journal of Food Biochemistry
Volume 2024, Article ID 6327916, 12 pages
https://doi.org/10.1155/2024/6327916

Research Article

Prediction of the Freshness of Grass Carp during Storage with Electric Nose Based on Signal Sequence Merging and Wavelet Transform

Guoqiang Zhao, Yuanyuan Chen, Mei Xie, Yihong Tan, Yong Jiang, and Li Zhao

School of Life Science, Jiangxi Science and Technology Normal University, Nanchang 330013, China

Correspondence should be addressed to Yong Jiang; 1020130968@jxstnu.edu.cn and Li Zhao; 1064590014@qq.com

Received 17 October 2023; Revised 4 December 2023; Accepted 15 April 2024; Published 23 April 2024

Academic Editor: Changmou Xu

In order to predict the freshness of grass carp, a novel data preprocessing method was proposed for electronic nose (E-nose) signals. The signal sequences from six sensors were selected and subsequently normalized. The direct signal sequence merging (DSSM) and reversed signal sequence merging (RSSM) modes were used for signal sequence merging. Subsequently, the genetic algorithm (GA) was used to evaluate the contribution of diverse sensors, and the merged data sequence was compressed using wavelet transform (WT). Using approximation coefficient and detail coefficient based on different scales and different signal sequence merging modes, principal component analysis (PCA) discriminated successfully storage time of chilled fish fillet. The PCA plots clearly demonstrated that all extracted feature data fully retain the signal characters. The partial least squares (PLS) and artificial neural network (ANN) models were used to establish prediction models for the freshness of grass carp during storage. The DSSM-ANN-A_5 and DSSM-PLS-D_4 models were chosen as the TVB-N content prediction models, while the DSSM-ANN-D_5 and RSSM-PLS-A_0 models were selected as the *K* value prediction models. The R^2 values of these models are higher than 0.9, and they have a good coefficient of determination. The results of this study suggest that it using E-nose signals to predict TVB-N content and *K* value is an effective method for assessing the freshness of grass carp during storage.

1. Introduction

A number of degradative reactions begin in the fish flesh after the death of a fish. These reactions are caused by chemical, biochemical, and microbial metabolic activity. Various components decompose and new compounds form during fish spoilage, resulting in changes to the perceived quality (odor, flavor, and texture) of the fish meat [1].

Freshness is very important when assessing the quality of fish and fishery products [2]. It can be described by various indicators based on biochemical changes after slaughter, including the *K* value [3], total volatile basic nitrogen (TVB-N) [4, 5], and thiobarbituric acid contents [6]. The *K* value, which measures the extent of the breakdown of adenosine triphosphate (ATP) in fish flesh [7], can be obtained by measuring inosine (HxR), hypoxanthine (Hx), ATP, adenosine diphosphate (ADP), adenosine monophosphate (AMP), and inosinic acid (IMP) with high-performance liquid chromatography (HPLC). A range of methods have been used to measure TVB-N since the measurement method was first described in Conway and Byrne [8]. Generally, the meat sample or an extract of meat is alkalized; the volatile bases are collected and titrated with acid, and then the total bases are calculated in accordance with the amount of acid. Moreover, chromatographic techniques such as GC-MS, SPME-GC-MS, and HPLC have produced convincing results and proved to be suitable for the determination of TVB-N [9–11]. However, these conventional methods are cumbersome, expensive, time-consuming, and destructive. Therefore, developing a convenient, cost-effective, rapid, sensitive, and reliable method for freshness determination is necessary.

In recent years, many studies have focused on developing rapid and nondestructive methods to evaluate the freshness of food. Among them, the electric nose (E-nose) is a system composed of a series of chemical sensors with specific response and appropriate pattern recognition algorithms, which can rapidly detect and recognize single or mixed complex gases while also providing comprehensive odor information for the tested sample [12]. Li et al. [4] developed simple mathematical models relating E-nose signals to variations in total viable count (TVC) and TVB-N for packaged pork during refrigerated storage. An input-modified convolution neural network combined with E-nose and hyperspectral imaging was utilized to evaluate TVB-N of mutton [5]. Furthermore, the prediction of *K* value with E-nose has also been reported in recent literature. Li et al. [3] predicted the freshness of horse mackerel by utilizing the E-nose, electronic tongue (E-tongue), and colorimeter combined with a data fusion strategy and different pattern recognition algorithms. The square correlation coefficient of the test set for the prediction model of *K* value was 0.936. Previous studies have successfully showcased the efficacy of E-nose in predicting the freshness of food. However, a significant portion of these studies focuses on selecting appropriate pattern recognition algorithms, especially deep learning algorithms, in recent years [13], to improve the accuracy of E-nose prediction for food freshness. For the E-nose, in addition to the pattern recognition algorithm, data processing plays an important role in improving the prediction accuracy.

The mean value or maximum value is typically used as a feature signal in the analysis of E-nose data [14, 15]. However, one sensor can only provide one kind of data, which may not necessarily correspond to characteristic responses. Consequently, acquiring more data necessitates the use of additional sensors, but increasing the number of sensors leads to more complex and expensive operations. Therefore, improving the data processing method is necessary to obtain majority of the response data from the E-nose and obtain higher prediction accuracy with fewer sensors. Li et al. [16] used discrete wavelet transform (WT) to extract important features from dynamic sensor responses and then evaluated egg storage time and yolk index with satisfactory predictions. This inspired us to think about a new idea for predicting the freshness of grass carp (*Ctenopharyngodon idella*) using an E-nose. The WT method can remove high frequency noise and compress data. Hence, the features can be selected for determining multicomponent samples by WT, and different wavelets give rise to different results. As a minute tool for time-frequency dynamic responses, WT has been applied in various fields [17–19]. Here, WT is tried as a new data processing method to extract feature signal from E-nose.

This paper presents a feature extraction method for the purpose of evaluating freshness of grass carp during 4°C storage using an E-nose effectively. Specifically, the measured signal sequences of the E-nose are merged and the features are extracted to obtain more useful information from the merged signal sequence as a feature signal by using the WT method. Then, combined with chemometric methods, both the TVB-N content and the *K* value can be predicted quantitatively.

2. Materials and Methods

2.1. Raw Material. Twenty grass carps were obtained from a local supermarket near the laboratory in Nanchang, China, and each fish weighed about 2–2.5 kg. These grass carps were killed by a sharp blow to the head, and then fish muscles were dissected carefully from the dorsal and ventral regions of the lateral line and weighed between 50 g and 55 g. Four fillets can be obtained from each grass carp. Immediately, these fillets were stored inside a plastic container at 4°C prior to determination.

Eight fillets were randomly taken out from the container on days 0, 2, 4, 6, 8, 10, 12, 14, and 16, respectively. Each fillet was homogenized for 1 min and then divided into three parts. One part of the samples was distributed for E-nose sample preparation, another part was used for *K* value measurement, and the remaining part was utilized for TVB-N content measurement.

2.2. TVB-N Content Measurements. The TVB-N content in the fillet was measured according to GB/T 5009.44 (2003). Each fillet sample was ground individually, and then 10 g of grounded sample was taken into a conical flask and impregnated with 100 mL distilled water for 30 min; the conical flask was often shaken before filtration to ensure uniform dispersion of the sample within the solution. Subsequently, 5 mL of filtrate was taken and blended with 5 mL of 10 g/L magnesia (MgO), distilled by a Kjeldahl distillation unit for 5 min. The distillate was absorbed with 10 mL of 20 g/L boric acid solution and titrated with 0.01 M of hydrochloric acid solution. The TVB-N content was calculated as shown in equation (1) by GB/T 5009.44 [20]:

$$\mathrm{X} = \frac{(V_1 - V_2) \times C \times 14}{m \times 5/100} \times 100. \quad (1)$$

In equation (1), X is the TVB-N content (mg/100 g), V_1 is the titration volume for the tested sample (mL), V_2 is the titration volume for the blank (mL), C is the concentration of HCl (mol/L), and m is the weight of ground fillet (g).

2.3. Determination of K Value with HPLC. The method for measuring the ATP-related compounds with HPLC was modified and validated based on the reference described by Barat et al. [21] and published in a Chinese journal [22].

Two grams of minced muscle were placed into a centrifuge tube and oscillated under vortex movement with 10 mL of 10% perchloric acid for 2 min and then centrifuged at 10,000 g under cold conditions (4°C) for 10 min. The supernatant was taken out, and the sediment was treated with 5.0 mL of 10% perchloric acid repeatedly. Repeat the operation once and put all supernatants together. The pH of the supernatant was adjusted to 6.5 with 1 mol/L sodium hydroxide solution. It was made up to/diluted to 50 mL with deionized water and filtered through a 0.45 mm membrane filter for further analysis.

HPLC analysis was performed by the Agilent 1260 high-performance liquid chromatography equipped with an UV-vis absorbance detector (Agilent Technologies, USA). ATP and its related compounds were separated in a Waters C18 column (4.6 mm i.d. ×150 mm, 5 μm). The mobile phase was triethylamine phosphate solution (3.5 mL of phosphoric acid solution and 7.2 mL of triethylamine solution was made up to 1,000 mL with deionized water, and pH was adjusted to 6.5 with triethylamine): methanol = 95 : 5. A sample (20 μL) was injected with a flow rate at 1 mL/min, and peaks were detected at 254 nm.

The amounts of ATP and its related compounds were determined and calculated based on the extra-calibration curves of standard ATP, ADP, AMP, IMP, HxR, and Hx. *K* value was defined by the following equation [7]:

$$\text{K value}\,(\%) = \frac{(\text{HxR}) + (\text{Hx})}{(\text{ATP}) + (\text{ADP}) + (\text{AMP}) + (\text{IMP}) + (\text{HxR}) + (\text{Hx})} \times 100. \quad (2)$$

2.4. Analysis of Aroma by Electronic Nose. A sensor array system (Gemini, Alpha M.O.S., France) with 6 metal oxide sensors was used to acquire the signal of aroma from minced muscle. The sensors were sensor T70/2 (Sensing species: toluene, xylene, carbon monoxide), sensor PA/2 (Sensing species: ethanol, ammonia, amine compounds), sensor P30/1 (Sensing species: hydrocarbons, ammonia, ethanol), sensor P40/2 (Sensing species: chlorine), sensor LY2/GH (Sensing species: ammonia, amine compounds), and sensor LY2/gCTL (Sensing species: hydrogen sulfide).

2 g minced fillet was placed in a 20 mL vial (Alltech, USA). The vials were sealed with a 20 mm silicone/PTFE magnetic crimp-top cap which was obtained from CNW Technologies GmbH (Dusseldorf, Germany). The vials were equilibrated for 30 min at 30°C. In the previous experiment, the incubation condition has been optimized. The response of the E-nose increased with the incubation temperature and time. The incubation temperature was selected to be 30°C because it is a normal temperature. The response increased quickly with time at 30°C and became slow after 30 min. So, this incubation condition was chosen. Then 1,000 μL of headspace gas was injected into the sensor chamber, and it was measured for 200 s, with a 0.5 s sampling interval. Dried air (purity 99.999%) was employed as the carrier gas, and the flow rate was 600 mL/min. After sample analysis, the system was purged for 300 s.

2.5. E-Nose Signal Pretreatment. The 101 data points (0–50 s) extracted from each sensor of E-nose are selected, and they are normalized between 0 and 1, respectively, by the following equation [23]:

$$\text{R} = \frac{R_i - \text{R}_{\min}}{R_{\max} - \text{R}_{\min}}, \quad (3)$$

where R: the normalized response; R_i: the response value at a sensor of E-nose; $R_{\min}$: the minimum response value at a sensor of E-nose; and $R_{\max}$: the maximum response value at a sensor of E-nose.

The merging signal sequence is compressed by WT before analyzing data with statistical techniques. The different Daubechies (dbN) wavelets and decomposition levels are used, and the optimum dbN mother wavelet and decomposition level are determined for the wavelet transform of E-nose signal.

2.6. Data Analysis. The genetic algorithm (GA) was performed to evaluate the influence of the diverse sensors on prediction of the *K* value. GA is a custom program written by Leardi, executed on Matlab [24]. The evaluation per run of the GA was set to 500, with 300 runs, while the remaining parameters were kept at their default values.

Compressed data were analyzed by partial least squares (PLS), artificial neural network (ANN), and principal component analysis (PCA). PLS was performed by means of the software SIMCA 14.1 (Umetrics, Umea, Switzerland); ANN and PCA were performed on Matlab 7.0 (MathWorks, Natick, MA, USA). PCA was applied to identify the different storage times of chilled grass carp fillet; ANN and PLS were employed to build predictive models for *K* value and TVB-N content with full cross-validation (leave-one-out cross-validation) approach. As for the performance of the established models, the evaluation indicator systems were mainly related to the square correlation coefficient (R^2) and root mean square error of cross-validation (RMSECV), respectively.

3. Results and Discussion

3.1. TVB-N Content and K Value Changes of Grass Carp during Storage. Figure 1 presents the changes of TVB-N content and *K* value of grass carp fillet during storage at 4°C. The TVB-N content of grass carp fillet increases as storage time increases as shown in Figure 1(a). The initial TVB-N content is 15.4 mg/100 g, and the final TVB-N content is 38.2 mg/100 g when the flesh decayed in the end. The TVB-N content on day 6 is 20.9 mg/100 g, which indicates that the fillet is beginning to decay. In addition, the error bars reveal that the relative standard deviation (RSD) of measured TVB-N content of each storage group is less than 5%.

The concept of the *K* value as a freshness indicator was introduced by Saito et al. [7]. The larger the *K* value is, the lower the freshness of the fish is. Generally, the *K* value of live fish is between 0 and 10, while *K* value of fresh fish is between 15 and 35. The fish flesh is not regarded as fresh when the *K* value is greater than 50 [6]. Figure 1 shows an

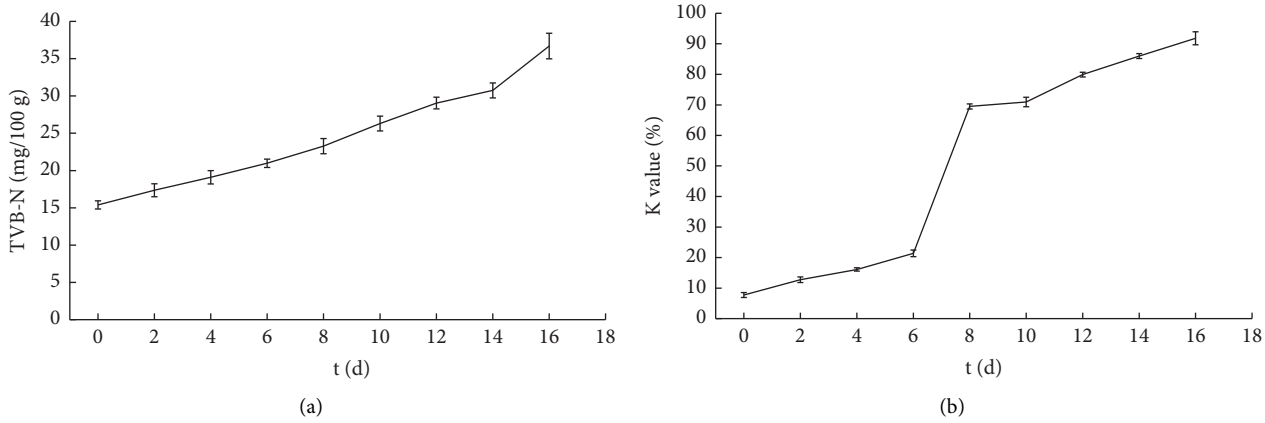

Figure 1: The changes of TVB-N content (a) and K value (b) of grass carp fillet during storage at 4°C.

almost linear increase in the K value of grass carp flesh during storage at 4°C. The initial K value is 7.72, and the K value is 91.81 when the flesh completely decayed in the end. However, the increase of the K value is significant from the sixth day to the eighth day of storage, and the K value exceeds the fresh threshold (50) after the sixth storage day. The RSD of measured K value of each storage group is less than 10%.

3.2. E-Nose Signal. The signals extracted from E-nose are shown in Figure 2(a). Each curve represents a different sensor response. They are denoted as T70/2, PA/2, P30/1, P40/2, LY2/Gh, and LY2/gCTL, respectively, according to their sensors. Different sensors have varying sensitivities to gas, resulting in differing responses from each electronic nose sensor, with some exhibiting higher responses than others. Figure 2(a) shows that signals from sensors (P30/1, P40/2, LY2/Gh, and LY2/gCTL) change little compared with the signal from other sensors. Hence, the enlarged signals are presented in Figures 2(b)–2(d).

Figure 2 shows that the responses of the six sensors vary a lot with time in the beginning of curve and stabilize gradually until the end of the measurement. Each curve contains much information. In most studies, each E-nose sensor only adopts one data point (mean value or max value of signal), and much useful information is wasted. In this paper, full utilization of information included in the signals of each E-nose sensor is attempted. A larger signal variability is observed at the initial period of the curve, indicating that this range may account for the majority of the original information. Therefore, a selection of 101 data points from the first 50 seconds signal of each sensor was selected as tentative character responses. However, it is crucial to extract feature signal sequences from these selected data points.

3.3. Evaluation of Diverse Sensors with GA. The GA was used to evaluate the contribution of diverse sensors to prediction. GA can simulate natural selection and evolution and find the optimal solution globally by searching through the entire solution space.

In dataset of GA, there is a one-to-one correlation between one direct signal sequence merging and one measured K value. After 300 runs, GA provided a total of 88 feature data points. The frequency of selection is shown in Figure 3. It can be observed that data points 304–308 and 345 have a high frequency of selection, indicating that data points acquired by P40/2 are more relevant to predicting the K value. The remaining feature data points, whose selected frequency is nearly equal, are distributed on diverse sensors. So, the data points from all six sensors must be used.

3.4. Merging E-Nose Signal Sequence. In Li et al. [16], WT was used to extract characteristic information from the sensor response of E-nose for evaluating egg storage time and yolk index. They decompose the original signal from each sensor, respectively, and obtain a series of coefficients sets. Then, new corresponding signal was reconstructed from the coefficient sets for qualitative and quantitative analysis.

Similarly, WT was adopted in this paper. However, Figure 2 shows that signal from different sensors differs significantly. Thus, each selected data sequence from different sensor has to be normalized according to equation (3) unlike the WT. These selected data sequences are denoted as T70/2, PA/2, P30/1, P40/2, LY2/Gh, and LY2/gCTL, respectively, according to their sensors. Two signal sequence merging modes are compared: the first mode is that normalized data sequences are merged from end to head as T70/2-PA/2-P30/1-P40/2-LY2/Gh-LY2/gCTL, shown in the top subgraph of Figure 4. This mode is referred to as direct signal sequence merging (DSSM). The beginning of each data sequence has a larger value compared to the end, so a sharp increase appears in the joining of two data sequences. The second mode is to reverse the normalized data sequences from the 3 sensors (PA/2, P40/2, LY2/gCTL), followed by combining them with the other three data arrays, with the linking sequence same as the DSSM mode. This mode is called the reversed signal sequence merging (RSSM) mode. The top subgraph of Figure 5 shows that the junctions of two

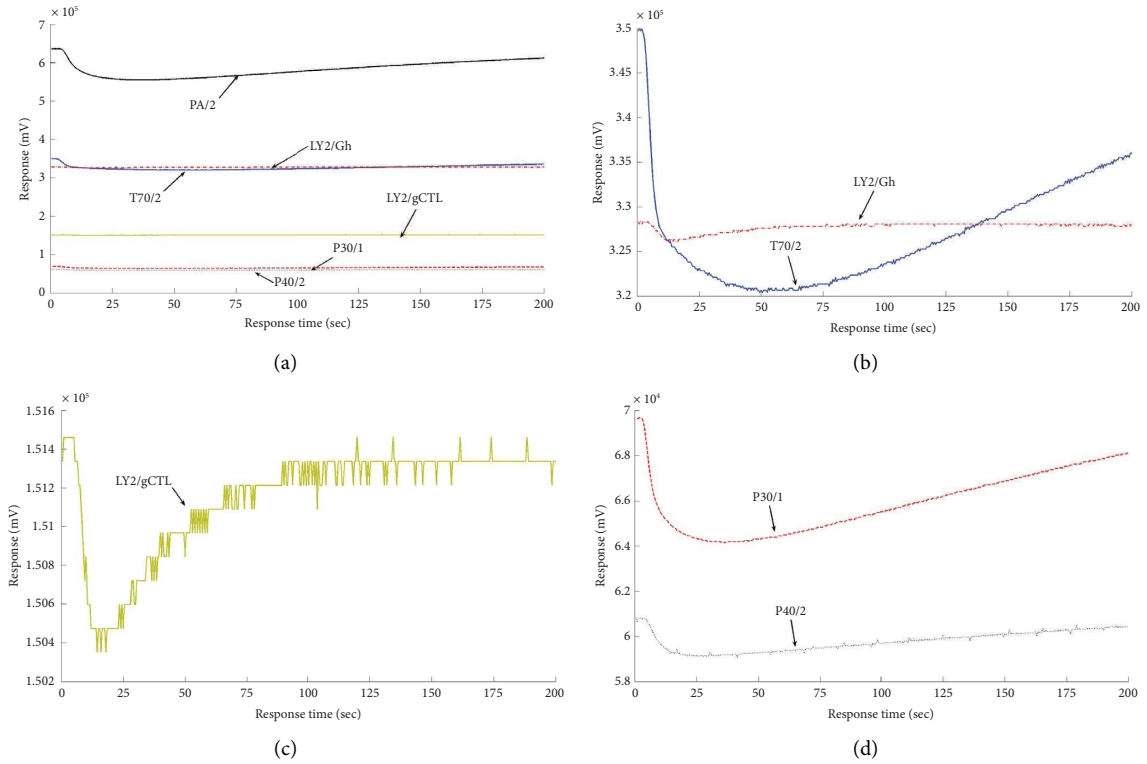

Figure 2: E-nose response curves of (a) six sensors, (b) LY2/Gh and T70/2 sensors, (c) LY2/gCTL sensor, and (d) P30/1 and P40/2 sensors from grass carp fillet on 0 day.

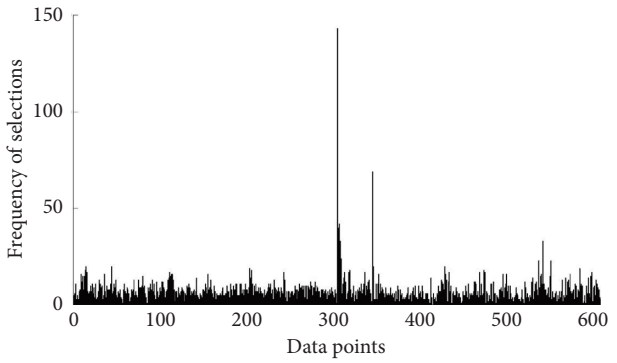

Figure 3: Frequency of selection of data points from direct merging signal sequence after 300 runs with GA.

data sequences of RSSM mode are smoother compared with the DSSM mode. These two signal sequence merging modes are adopted in the following data analysis in order to evaluate the effect of two merging modes on the prediction of K value and TVB-N content.

3.5. Extracting Feature Signal with WT. WT was developed for the analysis of a merged signal sequence with Matlab 7.0. The data compression process is used to reduce data size. Apart from data compression, WT is also expected to minimize noise and other unwanted contents present in the signal [25].

The merged signal sequence could be decomposed into two sets of coefficients with the best mother wavelet and scale. The coefficients are obtained by convolving the merged signal sequence with the low-pass filter for approximation and with the high-pass filter for detail. The coefficients contain a series of A_j set and a series of D_j set where A represents the approximation coefficients, D represents the detail coefficient, and j represents the level of decomposition. The A_j set and D_j set retain the low-frequency and high-frequency content of the signal, respectively. The different scales of the approximation coefficients and detail coefficient are shown in Figure 4 (DSSM mode) and Figure 5 (RSSM mode). There are 606 data points in A_0, and the number of data points reduces by half when the decomposition level increases by 1. Finally, the data size is reduced by WT, with only 19 data points in the A_5 and D_5 sequence.

In this study, the optimization of WT parameters is performed using different signal sequence merging modes, approximation coefficients, and detail coefficients of different scales. Meanwhile, several mother wavelets are tried and evaluated. The first-order wavelet transform of the Daubechies' family (db1) is selected as mother wavelet by comparing and computing different wavelet bases.

3.6. PCA. PCA has been widely applied in the fields of pattern recognition and multivariate calibration. The newly generative variables are utilized to represent the original ones after processing by PCA, which effectively simplifies

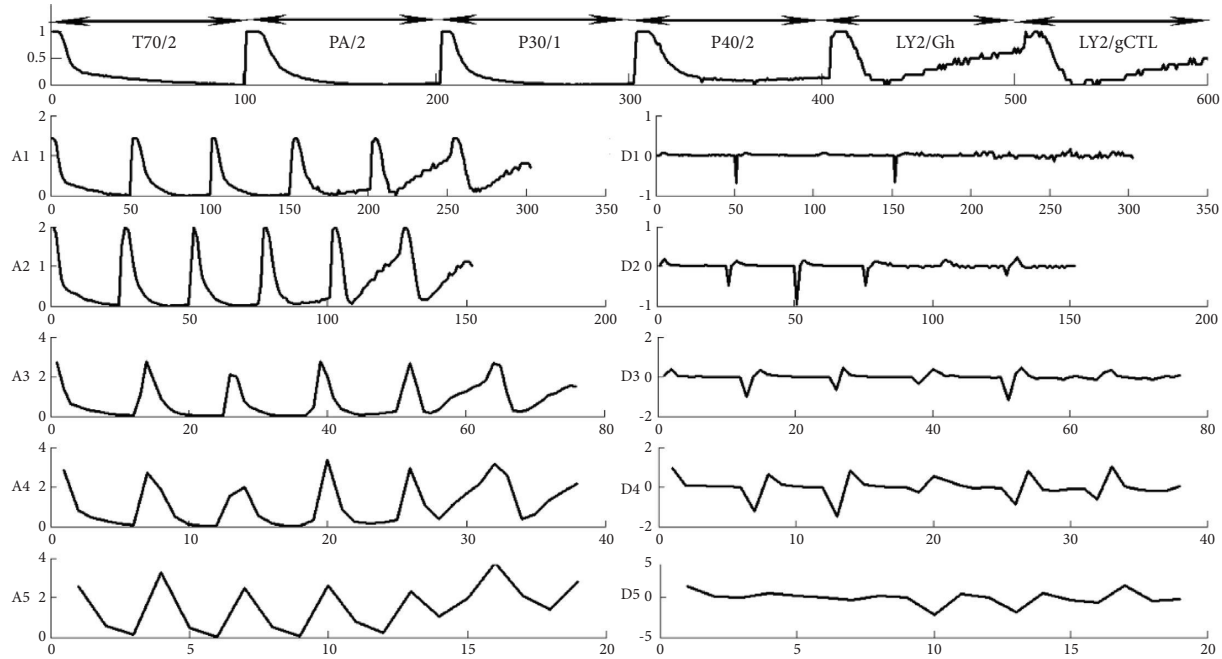

Figure 4: Direct merging signal sequence and its wavelet transform at all the five scales using db1. A_j represents approximation coefficients, D_j represents detail coefficient, and j represents the decomposition level.

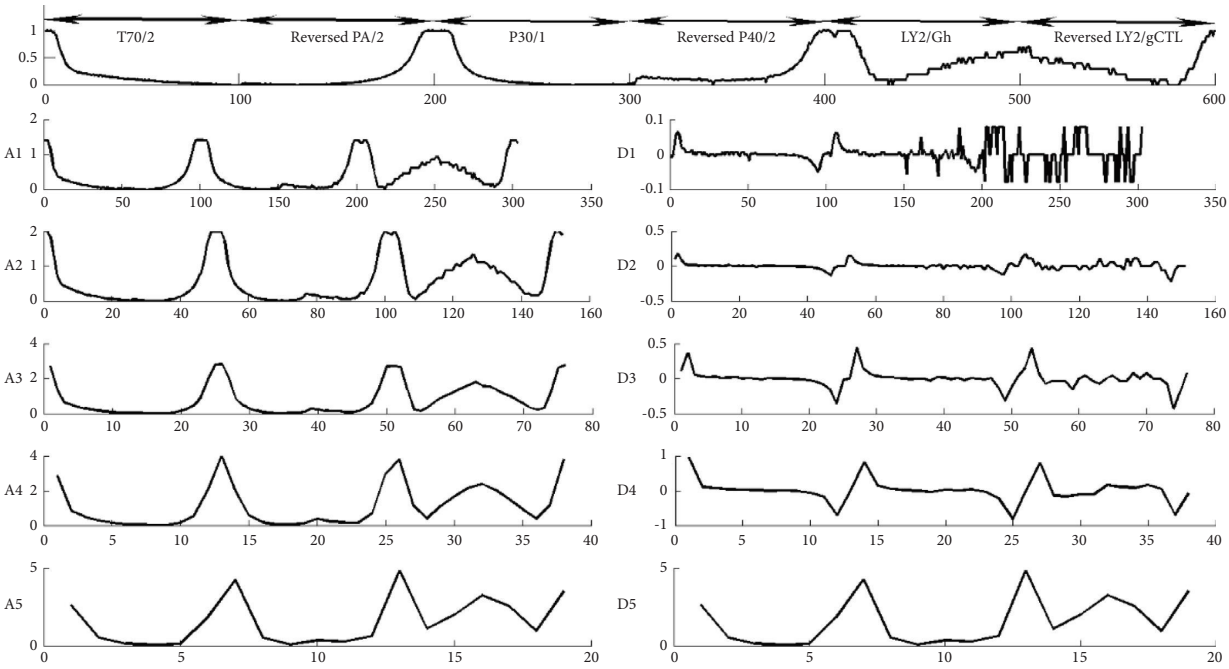

Figure 5: Reverse merging signal sequence and its wavelet transform at all the five scales using db1. A_j represents approximation coefficients, D_j represents detail coefficient, and j represents the decomposition level.

calculation. Samples can be grouped according to variance in principal component scores.

Figure 6 displays the two-dimensional PCA results of DSSM and RSSM modes for A_j sets and A_j sets based on WT. The arrangement of Figure 6 corresponds to Figures 4 and 5: PCA of A_0 is based on merged signal sequence, and PCA of each A_j or D_j is based on the A_j or D_j dataset obtained with WT, respectively.

The PCA plots of D-A_0, D-A_1, D-D_1, D-A_2, D-A_3, R-A_0, R-A_1, R-D_1, R-A_2, and R-A_5 exhibit similarities. The sample groups are clearly separated by PC1 within the first 8 days, decreasing along PC1. The samples from day 0 gather

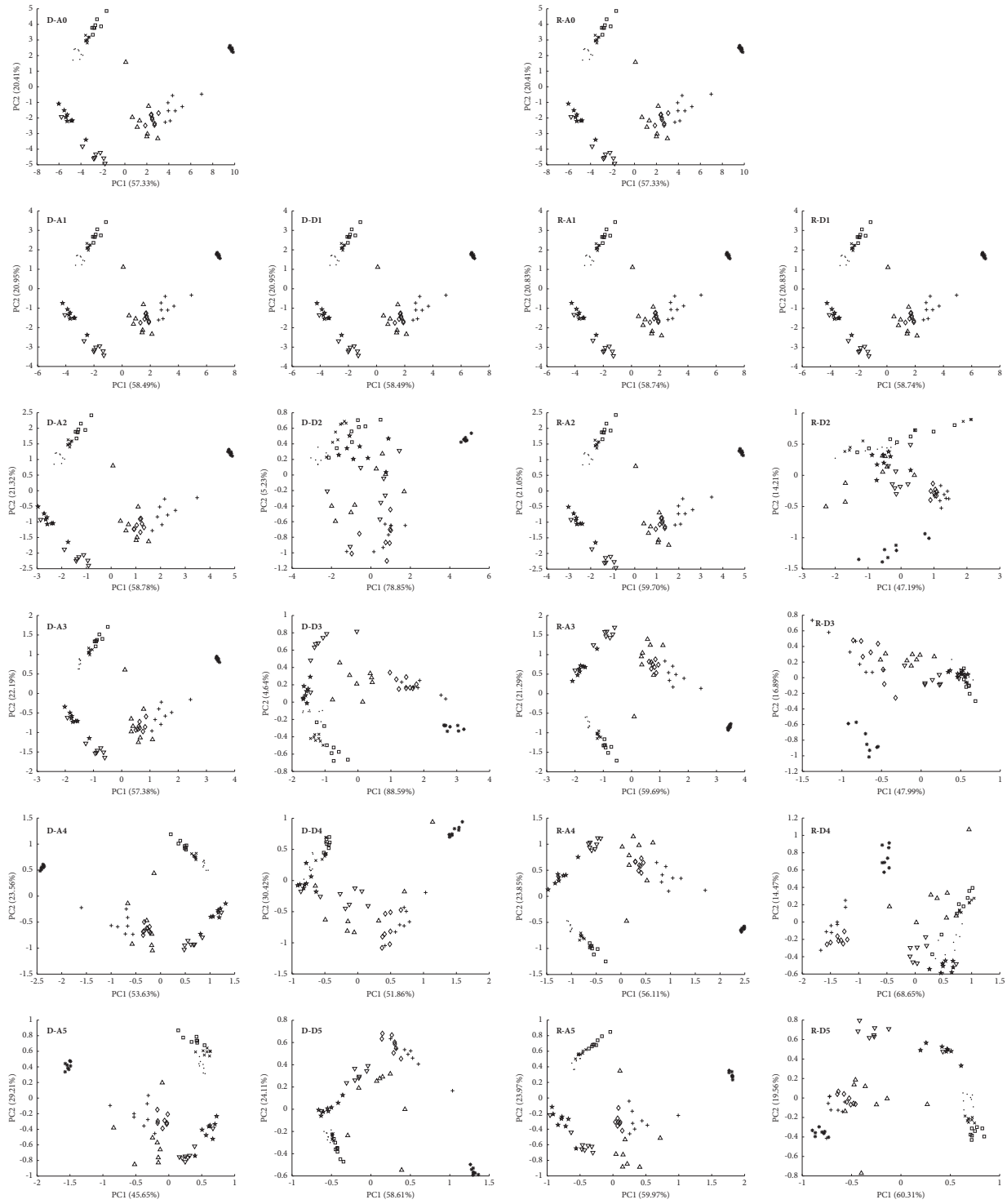

FIGURE 6: PCA plot of DSSM and RSSM modes analyzed with A_j and D_j sequences for grass carp fillet from different storage time (*: 0 d; +: 2 d; ◊: 4 d; ▽: 6 d; ⋆: 8 d; •: 10 d; △: 12 d; □: 14 d; ×: 16 d). A_j represents approximation coefficients, D_j represents detail coefficient, and j represents the decomposition level.

closely, while those from day 2 are more dispersed. The sample groups from day 6 to day 16 increase along PC2. Most sample groups are distinguished clearly except for a partial overlap between day 6 and day 10. The first two principal components (PC1 and PC2) explain 79.44% to 83.94% of the data variance. PCA plots of D-A_4, D-A_5, D-D_3, R-A_3, R-A_4, R-A_5, R-D_3, R-D_4, and R-D_5 also group most samples effectively, albeit with different arrangement. However, the D-D_2 and R-D_2 models showed no distinct grouping. The predictive effect of the K value and TVB-N content of grass carp flesh is compared by using the A_j sets and D_j sets based on WT with the ANN and PLS.

3.7. Prediction of K Value and TVB-N Content. The original data and all feature data from WT using approximation coefficients and detail coefficients of different scales are compared while doing analysis using PLS and ANN. PLS is positioned as a statistical technique for prediction renowned for their effectiveness in estimating structural equation models with latent variables [26]. ANN is a powerful, efficient, and nonlinear method with pattern recognition abilities, which makes it perfectly suited for the extraction of feature information from large data, especially due to complex biological, environmental, and instrumental variations [27]. Compared with other techniques, such as covariance and regression, ANN and PLS have better predictive ability and are frequently used in the prediction of texture, freshness, and safety of food [27–29]. For example, Basile et al. [27] employed nondestructive NIR spectroscopy and machine learning techniques to predict the texture parameters and total soluble solids content of grape. The results indicated that the multivariate models, created by constructing ANN and applying PLS regressions, displayed improved predictive capabilities following the removal of uninformative spectral ranges.

Several architectures of the network were investigated to predict the *K* value and TVB-N content. ANNs used in this paper are backpropagation (BP) and radial basis (RB) neural networks. The RB training algorithm is faster than BP for practical problems. The only optimized parameter is SPREAD. Despite various modifications to SPREDA, the predictive performance for both K value and TVB-N content remains subpar. It is proven that the RB model is not suitable in this study.

In this paper, the BP-ANN adopts the steepest gradient descent backpropagation training algorithm which updates the network weights and biases along the direction of the negative of the gradient. "Squashing" functions such as sigmoid transfer functions, that compress an infinite input range into a finite output range, are usually used in the hidden layers. If the input values are large, the gradient can have a very small magnitude and therefore cause small changes in the weights and biases, even though the weights and biases are far from their optimal values.

The PLS uses *X* (measured *K* value or TVB-N content) to construct a model of *Y* (predicted *K* value or TVB-N content), where the objective is to predict the latter from the former for new samples in the prediction set.

The two models are further evaluated with full cross-validation using a "leave-one-out" technique. RMSECV and R^2 were adopted to evaluate the prediction ability of *K* value and TVB-N content. The small RMSECV means the prediction model is better. As for R^2, the closer it is to 1, the better the model is. A model performs well when the value of R^2 is in the range of 0.82–0.90; the model performs inaccurately while the value of R^2 is lower than 0.82; and the value of R^2 higher than 0.90 shows excellent performance of the model.

3.7.1. TVB-N Content. The prediction results of PLS and ANN models based on signal sequence merging (DSSM and RSSM modes) and WT for TVB-N content are shown in Table 1. It is interesting that the prediction results with A_j sets are better in ANN models, in which the best model is the DSSM-A_3 model (R^2 is 0.9683, RMSECV is 1.6582 mg/100 g); on the contrary, the prediction results with D_j sets are better in PLS models, in which the best model is the DSSM-D_2 model (R^2 is 0.9685, RMSECV is 1.6521 mg/100 g). The best ANN and PLS models are based on the DSSM mode. Most values of R^2 are higher than 0.90, except for D_2 and D_3 models built with ANN. PLS, in addition to the RSSM-D_5 model, demonstrated strong performance in predicting TVB-N content, exceeding an R^2 of 0.9. Furthermore, no significant differences were observed between DSSM and RSSM models in predicting TVB-N content, except for a few models.

According to Table 1, the ANN model was built using the A_j sets, while the PLS model was built using the D_j sets. Figures 7(a)–7(d) visualize linear relationships between the predicted and measured TVB-N content with DSSM-ANN-A_3, DSSM-ANN-A_5, DSSM-PLS-D_2, and DSSM-PLS-D_4 models, respectively. The four models have a good coefficient of determination. Although R2 of the DSSM-ANN-A3 model is the highest in the ANN model, the R2 of DSSM-ANN-A5 model is still higher than 0.90 (R2 is 0.9474, RMSECV is 2.1423 mg/100 g). Thus, it can be inferred that the DSSM-ANN-A5 model retains the original signal features, with a dataset size of 19 data points significantly less than the 76 data points in the DSSM-ANN-A3 model. The gradient descent training algorithm in the ANN model was too slow for practical problems. It cost 8 h to complete a performance when using merged signal sequence with 606 data points, and the run time decreased with fewer data numbers. It only cost 31 and 5 min to complete a performance when using DSSM-ANN-A_3 and DSSM-ANN-A_5 models, respectively. Although the running time of PLS model based on SIMCA is almost not affected by the number of data points, compared with the DSSM-D_2 model, the DSSM-D_4 model can better distinguish the storage time of chilled fish fillets in PCA plots, and the R^2 of DSSM-PLS-D_4 model still exceeds 0.9 (R^2 is 0.9606, RMSECV is 1.8437). Finally, DSSM-ANN-A_5 and DSSM-PLS-D_4 models are selected as prediction models for measuring TVB-N content.

3.7.2. K Value. The prediction results of PLS and ANN models based on signal sequence merging (DSSM and RSSM modes) and WT for *K* value are shown in Table 2. PLS models consistently demonstrate highly beneficial prediction results, with all R^2 exceeding 0.9 and no influence observed on the R^2 due to varying coefficient sets or signal sequence merging modes. Furthermore, the best model is the RSSM-D_2 model (R^2 is 0.9898, RMSECV is 4.7357). The *K* value prediction models with A_j sets, as established by ANN, perform well except the A5 model, which exhibits a low R2 possibly due to the limited number of data points. On the other hand, excellent performance is exhibited by the *K* value prediction model with D_j sets in ANN models, except for D_1. In this case, the best model is the DSSM-D_4 model (R^2 is 0.9731, RMSECV is 7.6938). Compared with A_j set,

Table 1: Prediction results of PLS and ANN models based on signal sequence merging and WT for TVB-N content in grass carp fillet.

	DSSM				RSSM			
	ANN		PLS		ANN		PLS	
	R^2	RMSECV (mg/100 g)	R^2	RMSECV (mg/100 g)	R^2	RMSECV (mg/100 g)	R^2	RMSECV (mg/100 g)
A_0	0.9526	2.0350	0.9465	2.1411	0.8984	2.9174	0.9465	2.1411
A_1	0.9566	1.9592	0.9454	2.1638	0.9614	1.8627	0.9440	2.1899
A_2	0.9446	2.2275	0.9435	2.1998	0.9567	1.9608	0.9427	2.2149
A_3	**0.9683**	**1.6582**	0.9406	2.2541	0.9561	1.9777	0.9392	2.279
A_4	0.9404	2.3046	0.9296	2.4463	0.9574	1.9326	0.9343	2.3657
A_5	**0.9474**	**2.1423**	0.9257	2.5097	0.9598	1.8835	0.9227	2.5586
D_1	0.9459	2.1989	0.9454	2.1638	0.9445	2.1124	0.9440	2.1899
D_2	0.8727	3.5193	**0.9685**	**1.6521**	0.7886	4.7766	0.9432	2.2051
D_3	0.8641	3.6728	0.9538	1.9937	0.8663	3.5316	0.9420	2.2269
D_4	0.9304	2.4694	**0.9606**	**1.8437**	0.9171	2.7992	0.9505	2.0628
D_5	0.9127	2.7949	0.9275	2.4801	0.9151	2.7579	0.8839	3.1035

The four models demonstrate outstanding performance in TVB-N content predicition and were subsequently discussed collectively. R^2 and RMSECV are highlighted in bold to facilitate quick identification of the models by other researchers.

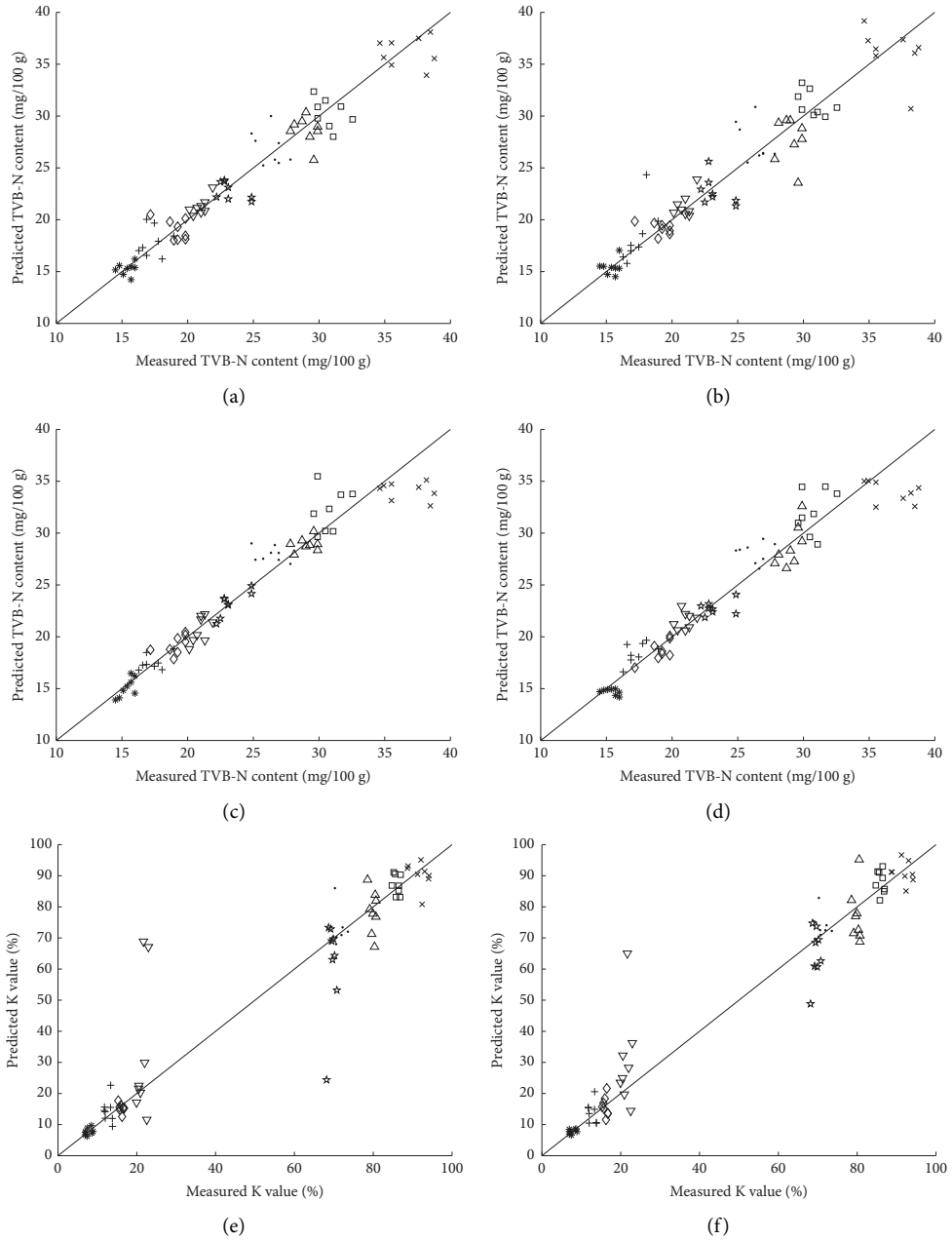

Figure 7: Continued.

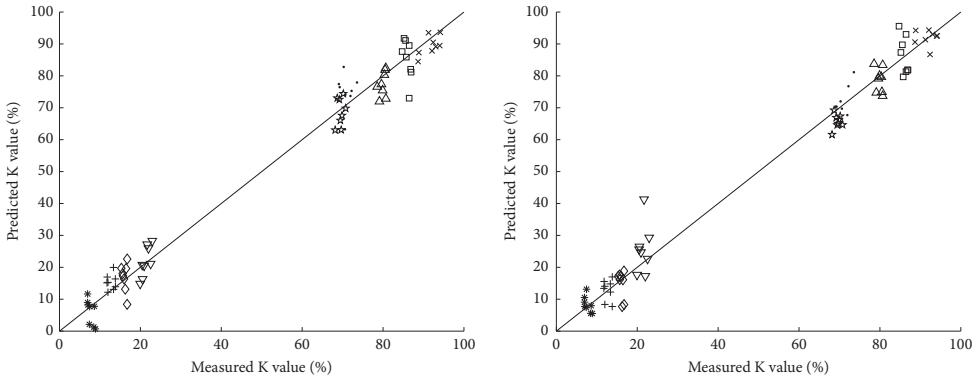

Figure 7: Predicted versus measured TVB-N content (a–c) and K value (d–f) for grass carp fillet from different storage time (*: 0 d; +: 2 d; ◊: 4 d; ▽: 6 d; ✶: 8 d; •: 10 d; △: 12 d;□: 14 d; ×: 16 d) analyzed by (a) DSSM-ANN-A_3 model, (b) DSSM-ANN-A_5 model, (c) DSSM-PLS-D_2 model, (d) DSSM-PLS-D_4 model, (e) DSSM-ANN-D_4 model, (f) DSSM-ANN-D_5 model, (g) RSSM-PLS-D_2 model, and (h) RSSM-PLS-A_0 model. The line is the line of equity ($y = x$).

Table 2: Prediction results of PLS and ANN models based on signal sequence merging and WT for K value in grass carp fillet.

	DSSM				RSSM			
	ANN		PLS		ANN		PLS	
	R^2	RMSECV (mg/100 g)	R^2	RMSECV (mg/100 g)	R^2	RMSECV (mg/100 g)	R^2	RMSECV (mg/100 g)
A_0	0.8860	15.5456	0.9897	4.7495	0.8828	15.594	**0.9897**	**4.7495**
A_1	0.8548	17.4384	0.9861	5.5128	0.8246	18.8033	0.9860	5.5232
A_2	0.9088	13.8726	0.9774	7.0117	0.8755	16.0485	0.9770	7.0811
A_3	0.9690	8.2243	0.9716	7.8500	0.9601	9.2765	0.9740	7.5217
A_4	0.9270	12.5095	0.9683	8.2817	0.9539	10.0793	0.9746	7.4355
A_4	0.7907	20.5730	0.9589	9.4117	0.7907	20.5730	0.9341	11.8435
D_1	0.8817	15.7388	0.9861	5.5128	0.8462	17.7255	0.986	5.5232
D_2	0.9695	8.3167	0.9882	5.0817	0.9525	10.1157	**0.9898**	**4.7357**
D_3	0.9375	11.5559	0.9829	6.1109	0.9573	9.6091	0.9841	5.9022
D_4	**0.9731**	**7.6938**	0.9602	9.2683	0.9623	9.0384	0.9670	8.4558
D_5	**0.9503**	**10.4359**	0.9402	11.2983	0.9612	9.2136	0.9361	11.6664

The four models demonstrate outstanding performance in K value predicition and were subsequently discussed collectively. R^2 and RMSECV are highlighted in bold to facilitate quick identification of the models by other researchers.

the K value prediction result with D_j sets in ANN model has better performance. Different from the TVB-N content prediction model, the performance of the K value prediction model is not significantly different between the DSSM and RSSM modes.

Figures 7(e)–7(h) visualize linear relationships between the predicted and measured K value with DSSM-ANN-D_4, DSSM-ANN-D_5, RSSM-PLS-D_2, and RSSM-PLS-A_0 models, respectively. Figures 7(d) and 7(e) indicate that the predicted K value is much greater than the measured K value on day 6, and greater deviations occur between predicted and measured K values on day 8. The reason is that the K value increases swiftly from day 6 (mean K value: 21.38) to day 8 (mean K value: 69.49) as shown in Figure 1(b). Parts of the samples may not be analyzed with HPLC and E-nose meantime. Measurement errors caused by analyzing time will be great. The DSSM-ANN-D_5 model, with fewer data points and R^2 great than 0.9 (R^2 is 0.9503, RMSECV is 10.4359), is selected as the K value prediction model. On the other hand, compared to the RSSM-PLS-D_2 model, the RSSM-PLS-A_0 model more effectively differentiates the storage time of chilled fish fillet in PCA plots, while still maintaining an R^2 greater than 0.9 ($R^2 = 0.9897$, RMSECV = 4.7495). Finally, DSSM-ANN-D_5 and RSSM-PLS-A_0 models are selected as prediction models for measuring K value.

In a similar work conducted by Huang et al. [14], the TVB-N content of pork meat was measured by integrating near infrared spectroscopy (NIRS), computer vision (CV), and E-nose techniques. PCA was employed to achieve data fusion, and the prediction model for TVB-N content was built using BP-ANN. The results revealed the outstanding performance of the data fusion model of NIRS, CV, and E-nose (RMSECV = 2.73 mg/100 g, $R^2 = 0.9527$). However, this method of data fusion is complex, expensive, time-consuming, and not suitable for rapid nondestructive testing requirements. Moreover, it is worth noting that the maximum response value response of each sensor was extracted as the characteristic variable, resulting in data waste. Consequently, the prediction performance of the E-nose model based on BP-ANN was found to be poor (RMSECV = 5.97 mg/100 g, $R^2 = 0.6495$).

Conversely, in this study, only an E-nose was used to measure chilled fish fillet, and an innovative electronic nose signal data preprocessing method was employed, which ultimately established excellent prediction models for the freshness of grass carp during storage.

4. Conclusions

In order to predict the freshness of chilled grass carp flesh, a signal pretreatment method was developed based on two types of signal sequence merging modes, with wavelet transform applied. The PCA analytical results reveal that the different scales and two kinds of signal sequence merging modes of approximation coefficients and detail coefficients can be used to distinguish the grass carp fillets of different storage time. In addition, successful utilization of PLS and ANN was achieved to build prediction model for measuring TVB-N content and K value of grass carp fillet. The DSSM-ANN-A_5 and DSSM-PLS-D_4 models are finally chosen as the TVB-N content prediction models, while the DSSM-ANN-D_5 and RSSM-PLS-A_0 models are finally selected as the K value prediction models. Even though the number of data points is reduced to 19 (A_5 and D_5) from 606 (A_0), they still show excellent performance of the model. There was no significant difference between the DSSM and RSSM models in the results of the established prediction model. This study proves that WT can condense and extract feature E-nose signal effectively. Not only can this E-nose signal preprocessing method be used to predict TVB-N content and K value, but it also has the potential capacity for other rapid determination with E-nose.

Data Availability

The data supporting the findings of this study are available from the corresponding authors upon reasonable request.

Conflicts of Interest

The authors declare that they have no conflicts of interest.

Authors' Contributions

Guoqiang Zhao was responsible for data curation, formal analysis, software, visualization, original draft preparation, and review and editing. Yuanyuan Chen was responsible for investigation, software, resources, and visualization. Mei Xie and Yihong Tan were responsible for investigation, resources, and visualization. Li Zhao and Yong Jiang were responsible for conceptualization, supervision, project administration, review and editing, and funding acquisition.

Acknowledgments

This study was supported financially by the Earmarked Fund for Jiangxi Agriculture Research System (Grant No. JXARS-[2023]-03) and Open Project of Aquatic Product Processing and Engineering Research Center of Safety Control of Jiangxi (No. KFJJ2301).

References

[1] L. Franceschelli, A. Berardinelli, S. Dabbou, L. Ragni, and M. Tartagni, "Sensing technology for fish freshness and safety: a Review," *Sensors*, vol. 21, no. 4, p. 1373, 2021.

[2] Z. Zhang, Y. Sun, S. Sang, L. Jia, and C. Ou, "Emerging approach for fish freshness evaluation: principle, application and challenges," *Foods*, vol. 11, no. 13, p. 1897, 2022.

[3] H. Li, Y. Wang, J. Zhang et al., "Prediction of the freshness of horse mackerel (Trachurus japonicus) using E-nose, E-tongue, and colorimeter based on biochemical indexes analyzed during frozen storage of whole fish," *Food Chemistry*, vol. 402, Article ID 134325, 2023.

[4] M. Li, H. Wang, L. Sun, G. Zhao, and X. Huang, "Application of electronic nose for measuring total volatile basic nitrogen and total viable counts in packaged pork during refrigerated storage," *Journal of Food Science*, vol. 81, no. 4, pp. M906–M912, 2016.

[5] C. Liu, Z. Chu, S. Weng et al., "Fusion of electronic nose and hyperspectral imaging for mutton freshness detection using input-modified convolution neural network," *Food Chemistry*, vol. 385, Article ID 132651, 2022.

[6] Z. Jia, C. Shi, J. Zhang, and Z. Ji, "Comparison of freshness prediction method for salmon fillet during different storage temperatures," *Journal of the Science of Food and Agriculture*, vol. 101, no. 12, pp. 4987–4994, 2021.

[7] T. Saito, K. Arai, and M. Matsuyoshi, "A new method for estimating the freshness of fish," *Nippon Suisan Gakkaishi*, vol. 24, no. 9, pp. 749-750, 1959.

[8] E. J. Conway and A. Byrne, "An absorption apparatus for the micro-determination of certain volatile substances: the micro-determination of ammonia," *Biochemical Journal*, vol. 27, no. 2, pp. 419–429, 1933.

[9] B. Bilgin and H. Gençcelep, "Determination of biogenic amines in fish products," *Food Science and Biotechnology*, vol. 24, no. 5, pp. 1907–1913, 2015.

[10] M. Sarmadikia, M. Mohammadi, A. Khezerlou, H. Hamishehkar, and A. Ehsani, "Effect of microencapsulated bitter orange peel extract in coatings based on quince seed mucilage on the quality of rainbow trout fillets," *Journal of Food Measurement and Characterization*, vol. 16, no. 5, pp. 3877–3887, 2022.

[11] K. Xu, Y. Yi, J. Deng et al., "Evaluation of the freshness of rainbow trout (*Oncorhynchus mykiss*) fillets by the NIR, E-nose and SPME-GC-MS," *RSC Advances*, vol. 12, no. 19, pp. 11591–11603, 2022.

[12] P. Liu and K. Tu, "Prediction of TVB-N content in eggs based on electronic nose," *Food Control*, vol. 23, no. 1, pp. 177–183, 2012.

[13] X. Ren, Y. Wang, Y. Huang et al., "A CNN-based E-nose using time series features for food freshness classification," *IEEE Sensors Journal*, vol. 23, no. 6, pp. 6027–6038, 2023.

[14] L. Huang, J. Zhao, Q. Chen, and Y. Zhang, "Nondestructive measurement of total volatile basic nitrogen (TVB-N) in pork meat by integrating near infrared spectroscopy, computer vision and electronic nose techniques," *Food Chemistry*, vol. 145, pp. 228–236, 2014.

[15] P. Li, Z. Ren, K. Shao, H. Tan, and Z. Niu, "Research on distinguishing fish meal quality using different characteristic parameters based on electronic nose technology," *Sensors*, vol. 19, no. 9, p. 2146, 2019.

[16] J. Li, S. Zhu, S. Jiang, and J. Wang, "Prediction of egg storage time and yolk index based on electronic nose combined with

chemometric methods," *LWT- Food Science and Technology*, vol. 82, pp. 369–376, 2017.

[17] J. Qiao, G. Su, C. Liu et al., "Study on the application of electronic nose technology in the detection for the artificial ripening of crab apples," *Horticulturae*, vol. 8, no. 5, p. 386, 2022.

[18] W. Qiao, Y. Wang, J. Zhang, W. Tian, Y. Tian, and Q. Yang, "An innovative coupled model in view of wavelet transform for predicting short-term PM10 concentration," *Journal of Environmental Management*, vol. 289, Article ID 112438, 2021.

[19] T. Wang, C. Lu, Y. Sun, M. Yang, C. Liu, and C. Ou, "Automatic ECG classification using continuous wavelet transform and convolutional neural network," *Entropy*, vol. 23, no. 1, p. 119, 2021.

[20] GB/T 5009.44-2003, *Method for Analysis of Hygienic Standard of Meat and Meat Products*, 2003.

[21] J. M. Barat, L. Gil, E. García-Breijo et al., "Freshness monitoring of sea bream (*Sparus aurata*) with a potentiometric sensor," *Food Chemistry*, vol. 108, no. 2, pp. 681–688, 2008.

[22] A. Fu, Y. Zhang, Y. Gao, Y. Zhou, and Y. Jiang, "Optimization method of K-Value and discussion its change about grass carp under cold storage condition," *Food Science and Technology*, vol. 42, no. 12, pp. 142–146, 2017.

[23] P. C. Slorach, H. K. Jeswani, R. Cuéllar-Franca, and A. Azapagic, "Environmental sustainability in the food-energy-water-health nexus: a new methodology and an application to food waste in a circular economy," *Waste Management*, vol. 113, pp. 359–368, 2020.

[24] R. Leardi, "Genetic algorithms in chemistry," *Journal of Chromatography A*, vol. 1158, no. 1-2, pp. 226–233, 2007.

[25] R. Banerjee, B. Tudu, L. Shaw, A. Jana, N. Bhattacharyya, and R. Bandyopadhyay, "Instrumental testing of tea by combining the responses of electronic nose and tongue," *Journal of Food Engineering*, vol. 110, no. 3, pp. 356–363, 2012.

[26] J. Evermann and M. Tate, "Comparing out-of-sample predictive ability of PLS, covariance, and regression models," 2014, http://aisel.aisnet.org/icis2014/proceedings/GeneralIS/23/.

[27] T. Basile, A. D. Marsico, and R. Perniola, "Use of artificial neural networks and NIR spectroscopy for non-destructive grape texture prediction," *Foods*, vol. 11, no. 3, p. 281, 2022.

[28] S. Grassi, S. Benedetti, L. Magnani, A. Pianezzola, and S. Buratti, "Seafood freshness: E-nose data for classification purposes," *Food Control*, vol. 138, Article ID 108994, 2022.

[29] M. K. D. Rambo, M. M. C. Ferreira, P. M. de Melo, C. C. Santana Junior, D. A. Bertuol, and M. C. D. Rambo, "Prediction of quality parameters of food residues using NIR spectroscopy and PLS models based on proximate analysis," *Food Science and Technology*, vol. 40, no. 2, pp. 444–450, 2020.